SARS-CoV-2 NSP13 suppresses the Hippo pathway downstream effector YAP

Fansen Meng[1], Jong Hwan Kim[2], Chang-Ru Tsai[3], Jun Wang[2], Yufeng Shi[2], Vaibhav Deshmukh[3], Xiao Li[1], Jeffrey Steimle[3], Bing Xie[3], Rich Li[1], James F. Martin[1,2,3*]

[1]McGill Gene Editing Lab, The Texas Heart Institute; 6770 Bertner Avenue, Houston, Texas, 77030, USA.

[2]Cardiomyocyte Renewal Laboratory, The Texas Heart Institute; 6770 Bertner Avenue, Houston, Texas, 77030, USA.

[3]Department of Integrative Physiology, Baylor College of Medicine; One Baylor Plaza, Houston, Texas, 77030, USA.

[*]James F. Martin. Tel: +1 713 798 5931, e-mail: jfmartin@bcm.edu.

Abstract: The Hippo pathway plays critical roles in tissue development, regeneration, and immune homeostasis. The widespread pandemic of Coronavirus disease 2019 (COVID-19) caused by SARS-CoV-2 has resulted in a global healthcare crisis and strained health resources. How SARS-CoV-2 affects Hippo signaling in host cells has remained poorly understood. Here, we report that SARS-CoV-2 infection in patient lung cells and cardiomyocytes derived from human induced pluripotent stem cells (iPS-CMs) suppressed YAP target gene expression, as evidenced by RNA sequencing data. Furthermore, in a screening of nonstructural proteins from SARS-CoV-2, nonstructural protein 13 (NSP13) significantly inhibited YAP transcriptional activity independent of the YAP upstream suppressor kinase Lats1/2. Consistent with this, NSP13 suppressed active YAP (YAP5SA) in vivo, whereby NSP13 expression reverted the phenotype of YAP5SA transgenic mice. From a mechanistic standpoint, NSP13 helicase activity was shown to be required for its suppression of YAP. Furthermore, through the interaction of NSP13 with TEAD4, which is the most common YAP-interacting transcription factor in the nucleus, NSP13 recruited endogenous YAP suppressors such as CCT3 and TTF2 to inactivate the YAP/TEAD4 complex. These findings reveal the function and mechanism of the SARS-CoV-2 helicase NSP13 in host cells and partially explain the toxic effect of SARS-CoV-2 in particular host tissue with high YAP activity.

Key words:

SARS-CoV-2, NSP13, Hippo pathway, YAP, TEAD4

Main Text:

INTRODUCTION

The evolutionarily conserved Hippo signaling pathway inhibits cell proliferation. When active, the Hippo pathway kinases Lats1/2 phosphorylate and inactivate YAP and TAZ, which are the two transcriptional coactivators and downstream effectors of the Hippo signaling pathway (*1, 2*). During the last twenty years, the critical roles of Hippo-YAP signaling in regeneration, development, diseases, and the immune homeostasis of organs, such as heart (*2, 3*), liver (*4*), intestine (*5*), and kidney (*6*), have been well established (*7, 8*). Dysregulation of Hippo signaling causes various diseases, including cancer and immune dysfunction. Recently, the global COVID-19 pandemic caused by severe acute respiratory syndrome coronavirus 2 (SARS-CoV-2) significantly affected the lives of billions of individuals. Besides its impact on the respiratory tract, increasing clinical evidence has indicated that COVID-19 affects multiple organs system, such as the digestive system, central nervous system, urinary system, and cardiovascular system (*9-12*). To date, molecular studies on SARS-CoV-2 have primarily focused on the antiviral response in host cells (*13-22*). However, the effect of SARS-CoV-2 on cell signal transduction is not well understood. Therefore, studying how SARS-CoV-2 affects Hippo signaling regulation may reveal more about the molecular basis of SARS-CoV-2–induced pathophysiology.

A member of the coronavirus family, SARS-CoV-2 is a positive-sense single-stranded RNA virus. The SARS-CoV-2 genome encodes as many as 14 open-reading frames and can be processed into 16 nonstructural proteins (NSP1–NSP16), 4 structural proteins (spike, envelope, membrane, and nucleocapsid), and 9 putative accessory factors (*23*). When SARS-CoV-2 enters into cells, spike protein binds to the transmembrane angiotensin-converting enzyme 2 (ACE2), and transmembrane serine protease 2 (TMPRSS2) primes the spike for entry. Then, the SARS-

CoV-2 genome is released into the host cell cytoplasm, initiating a complex program of viral gene expression (*24*). Host–virus protein–protein interactions are critical for the life cycle of a virus and for uncovering potential drug targets. Several groups have reported host cell SARS-CoV-2 interactomes obtained by using different strategies (*25*), such as affinity purification (*23, 26-29*), proximity labeling (*28, 30-34*), and a yeast two-hybrid system (*35*). These interactome data are critical for revealing the mechanisms underlying the pathogenesis and the clinical progression of COVID-19, as well as for developing antiviral therapies. However, these recourse data have not been validated, and how SARS-CoV-2 proteins affect Hippo signaling in host cells remains largely unknown.

Here, we report that SARS-CoV-2 infection inhibited YAP target gene expression in patient lung epithelial cells (AT1) and hiPS-CMs. In a screening of SARS-CoV-2 nonstructural proteins, we found that NSP13 significantly suppressed YAP transactivation independent of the YAP upstream suppressor Lats1/2. We further showed that NSP13 introduction in mouse CMs reversed the phenotype of heart failure, prevented heart overgrowth, and increased the survival rate in YAP5SA transgenic mice. Moreover, NSP13 suppressed YAP activity in a manner dependent on its helicase activity and nucleic acid–binding ability. Mechanistically, we found that NSP13 directly interacted with YAP transcription partner TEAD4 and that this interaction restrained the function of the YAP/TEAD4 complex by recruiting suppressors such as CCT3, CCT4, and TTF2. These findings reveal a novel function of NSP13 in the regulation of Hippo signaling, providing key insights into the pathogenesis of SARS-CoV-2.

RESULTS

SARS-CoV-2 infection suppresses YAP activity

To investigate alterations in the YAP activity of host cells after SARS-CoV-2 infection *in vivo*, we integrated and reanalyzed the single cell or single nuclei RNA (scRNA/snRNA) sequencing data from lung samples of donors who died from COVID-19 (*36, 37*) (**Fig. 1A** and **fig. S1A**). As recently reported, SARS-CoV-2 primarily attacks cells expressing SARS-CoV-2 entry factors, such as SARS-CoV-2 spike receptor ACE2 and serine protease TMPRSS2, which facilitate SARS-CoV-2 infections by cleaving and priming the spike protein of SARS-CoV-2 (*38-41*). Lung epithelial cells have a higher expression of TMPRSS2 and ACE2 than other cells in lung (**Fig. 1B** and **fig. S1B**) and are therefore vulnerable to SARS-CoV-2 infection. Patient lung epithelial cells were divided into two groups: alveolar type 1 (AT1) and alveolar type 2 (AT2) cells (**Fig. 1C and fig. S1C**). Because AT1 cells cover more than 95% of the alveolar surface and have higher TMPRSS2 expression than AT2 cells do (**Fig. 1C**), SARS-CoV-2 is more likely to infect AT1 cells. Intriguingly, the YAP score evaluated by for hundreds of YAP target genes was decreased in AT1 cells from patients with COVID-19 when compared with control (**Fig. 1D**), indicating that SARS-CoV-2 infection suppressed YAP activity. Previous studies have shown that YAP activity is important for maintaining AT1 cell identity (*42, 43*). Consistent with this and the reduced YAP score in AT1 cells, AT1 cell signature genes, such as *AGER*, *HOPX*, and *CLIC5,* were downregulated in lung samples from patients with COVID-19, along with canonical YAP target genes such as *TEAD1*, *PALLD*, *LATS2*, *AMOTL2,* and *TIMP2* (**fig. S1D**). Importantly, the reduced YAP activity observed after SARS-CoV-2 infection in AT1 cells may be partially responsible for the reduced lung function observed in patients with COVID-19 (*36, 37*).

To further support that direct infection with SARS-CoV-2 suppresses YAP activity in host cells, we performed an independent analysis on previously reported bulk RNA-seq data obtained from human induced pluripotent stem cells iPSC-derived cardiomyocytes (CMs) infected with varying doses of the SARS-CoV-2 virus (*44*). Compared with mock infection CMs, SARS-CoV-2–infected CMs exhibited a dose-dependent upregulation of the *pp1ab* transcript (precursor of *nsp13* RNA) (**fig. S1E**), confirming the findings reported in the paper. Subsequently, we evaluated the average expression of 302 previously reported CM-specific YAP target genes (*45*) in the iPSC-CM RNA-seq dataset. Our analysis revealed that YAP target genes were most highly expressed in the mock infection group, with their expression significantly decreasing in a dose-dependent manner in CMs infected with SARS-CoV-2 virus (**Fig. 1E)**. To illustrate this finding, we have shown expression data for several canonical YAP targets in CMs, including *VGLL3*, *AMOTL2*, *CCN1,* and *CCN2*, demonstrating their reduced expression in the virus-infected iPSC-CMs (**Fig. 1F)**. These data support that SARS-CoV-2 infection suppresses YAP activity in host cells.

NSP13 inhibits YAP5SA *in vitro*

To explore which SARS-CoV-2 protein suppresses YAP activity, we screened 11 NSP proteins by using a dual-luciferase reporter assay. Compared with other NSPs, NSP13, albeit at low protein expression levels, strongly inhibited YAP transcription activity (**Fig. 2A**). The highly conserved helicase NSP13 plays an essential role in viral replication and transcription, which makes it a promising target for developing pan-coronavirus therapeutics (*46-53*). Previously reported proximity-labeling data indicated that NSP13 directly interacts with Lats2 (*25*), suggesting that NSP13 may inactivate YAP by recruiting or activating its upstream kinase. To test this hypothesis, we examined the effect of NSP13 on constitutively active YAP (YAP5SA), which is resistant to

phosphorylation and inactivation by its upstream kinase Lats1/2 (*54*). Our reporter assay results indicated that NSP13 similarly suppressed YAP5SA transactivation (**fig. S2A**), suggesting that NSP13 has a Lats1/2-independent role in YAP suppression. Moreover, NSP13 attenuated YAP5SA activity in a dose-dependent manner, as revealed by studies performed by using another reporter plasmid (8*GTIIC_Luc) with a different promoter (**Fig. 2B**). To further investigate the specific effect of NSP13 on YAP activity, we used Notch reporter plasmids and found that NSP13 had no effect on Notch signaling (**fig. S2B**). Together, our findings show that NSP13 specifically suppresses YAP transactivation independent of Lats1/2 activity.

NSP13 inhibits YAP5SA *in vivo*

As we previously described (*45*), YAP5SA mice (aMyHC-MerCreMer;YAP5SA) expressing YAP5SA in CMs after tamoxifen (TAM) injection display CM hyperplasia and hypercellularity in the overall heart, which results in increased ejection fraction and fractional shortening. To explore the functional consequences of NSP13 expression in these mice *in vivo*, we constructed an adenovirus expressing NSP13 (AAV9-NSP13) that specifically infects CMs in the mouse heart. In a pilot experiment, NSP13 was highly expressed in WT mice around 12 days after infection with AAV9-NSP13 virus (**Fig. 2C**). The experimental design for further testing the function of NSP13 in YAP5SA mice is shown in **Figure 2D**. Both Control (aMyHC-MerCreMer;WT) and YAP5SA (aMyHC-MerCreMer;YAP 5SA) mice were injected with AAV9-GFP or AAV9-NSP13. At 12 days after virus injection, the mice were given two shots of low-dose TAM (10 ug/g). At days 4, 8, and 14 after the second shot of TAM, the cardiac function of mice was recorded by using echocardiography. No obvious body or behavioral changes were observed among the four groups of mice, indicating that NSP13 expression in CMs did not affect adult mouse health.

Consistent with our previous study findings, we found that YAP5SA mice started to die on day 8 after TAM injection as a result of heart failure (*45*) (**Fig. 2E**). As expected, NSP13 expression in CMs of YAP5SA mouse hearts significantly increased the survival rate and reversed the heart failure phenotype of these mice, as shown by increased ejection fraction (EF) and fractional shortening (FS) (**Fig. 2E-F and fig. S2C**). Moreover, NSP13 expression reversed the YAP5SA mouse phenotypes of a small left ventricle chamber, as shown by increased end-diastolic volume, diastolic left ventricle diameter, and systolic left ventricle diameter (*45*) (**Fig. 2G-H and fig. S2D-E**).

The survival data in **Fig. 2E** show that 40% (4/10) of YAP5SA-GFP mice and 80% (8/10) of YAP5SA-NSP13 mice survived to day 21 after TAM injection. To further examine the effects of NSP13 on the mouse heart, we collected heart tissues from the surviving mice. Intriguingly, the hearts of surviving YAP5SA mice were substantially larger than those of control mice because of CM proliferation, as indicated by the heart/body ratio and hematoxylin and eosin staining (**Fig. 2I and 2J**). Consistent with our *in vitro* data showing that NSP13 suppresses YAP5SA activity, NSP13 expression in YAP5SA mice prevented YAP5SA transactivation and reversed the overgrowth of heart (**Fig. 2I and fig. S2F**). Overall, these data support that NSP13 suppresses YAP activity *in vivo*.

NSP13 helicase activity is required for its suppression of YAP

We next examined how NSP13 suppresses YAP activity. NSP13 is a helicase with sequence conservation among all coronaviruses (**Fig. 3A**) and plays a critical role in viral replication. Therefore, NSP13 has been identified as a target for antiviral treatment. In a recent study of SARS-CoV NSP13, K131, K345/K347, and R567 were identified as important amino acid sites for

NSP13 helicase activity (*55*). Because SARS-CoV-2 NSP13 shares 99.8% sequence identity with SARS-CoV NSP13, (a difference of one single residue), we have presumed that these sites are similarly critical for SARS-CoV-2 NSP13. To investigate the mechanism for how NSP13 suppresses YAP activity, we constructed SARS-CoV-2 NSP13 mutant plasmids as previously described (*55*). Reporter assay results indicated that the suppression of YAP activity was preserved between wild-type NSP13 and NSP13-K131A, which has lower helicase activity. However, compared with wild-type NSP13, NSP13-K345A/K347A, which provides two additional hydrophobic alanine residues to block the entrance of nucleic acid binding channel, or NSP13-R567A, which prevents ATP consumption, resulted in the reduced suppression of YAP activity (**Fig. 3B**). These findings suggested that the binding of NSP13 with DNA or DNA/RNA and the unwinding of DNA or DNA/RNA by NSP13 are required for NSP13 to suppress YAP transactivation.

Notably, NSP13-K345A/K347A mildly increased YAP5SA transactivation. NSP13 consists of 5 domains: an N-terminal zinc binding domain (ZBD), a helical "stalk" domain (S), a beta-barrel 1B domain, and two "RecA like" helicase subdomains 1A and 2A that contain the residues responsible for its nucleotide binding and hydrolysis functions. To further evaluate the function of each domain on YAP, we constructed 7 NSP13 truncations on the basis of the NSP13 domain map (**Fig. 3C**). As shown in **Fig. 3D**, none of the truncations resulted in reduced YAP transactivation, but the 1A and 2A domains mildly enhanced YAP activity similar to NSP13 K345A/K347A, suggesting that the NSP13 nucleotide binding domain (1A or 2A) may interact with endogenous YAP suppressor(s) and prevent it (them) from interacting with YAP. Taken together, our data indicate that NSP13 suppresses YAP in a manner dependent on its helicase activity and may recruit endogenous YAP suppressors.

NSP13 mutants from SARS-CoV-2 variants had no effect on NSP13's suppression of YAP

SARS-CoV-2 has consistently mutated over time, resulting in variants that differ from the original SARS-CoV-2 virus. As shown in Fig. 3E, all the NSP13 mutations from SARS-CoV-2 variants are summarized, including Q88H, D260Y, E341D, R392C, and P419S (**Fig. 3E**), and their location has been shown on the published NSP13 protein structure model (PDB:7NN0) (*49*) (**fig. S3A**). The structural data indicated that none of the mutations from SARS-CoV-2 variants had any influence on the ability of SARS-CoV-2 to consume ATP and bind nucleic acids (**fig. S3A**), with the exception of R392C. This mutation came from the omicron variant and, given that it resides on the interface between NSP13 and DNA, may affect its binding with DNA (*49*). We then constructed NSP13 mutant plasmids and tested the function of NSP13 mutations on YAP. As shown in **Fig. 3F** and **fig. S3B**, similar to wild-type NSP13, NSP13 mutants from SARS-CoV-2 variants suppressed YAP transactivation. R392C from the omicron variant had no effect on DNA binding, given that NSP13-R392C inhibited YAP.

NSP13 interacts with the YAP/TEAD complex in the nucleus

Because NSP13 protein may suppress active YAP *in vivo* by directly suppressing YAP transactivation or by affecting YAP5SA expression, we examined NSP13 and YAP5SA expression in mouse hearts 3 days after TAM injection using western blot (WB) and immunofluorescence (IF) studies (**fig. S4A**). As shown in **fig. S3B-C**, YAP5SA protein levels were similar between the GFP and NSP13 groups, indicating that NSP13 inhibited YAP5SA activity by suppressing its transactivation but not by affecting protein expression or mediating degradation, which is consistent with our other *in vitro* data (**fig. S2A**).

We next explored the molecular mechanism for how NSP13 suppresses YAP. IF data revealed that NSP13 localized in cytoplasm and nucleus, whereas most of YAP5SA colocalized with NSP13 in the nucleus at 3 days after TAM injection (**Fig. 4A** and **fig. S4C**), suggesting that NSP13 suppresses YAP transcriptional activity in the nucleus. However, co-immunoprecipitation (co-IP) experiments suggested no direct interaction between NSP13 and YAP5SA (**fig. S4D**). Further results indicated that NSP13 associated with YAP's interaction partner TEAD4, which is a transcription factor in the nucleus (**Fig. 4B**). This finding implies that NSP13 may prevent YAP transactivation by competitively interacting with TEAD4, thereby disrupting the YAP/TEAD4 complex. The AlfaFold model predicted that both the N- and C-terminal ends of TEAD4 interacted with NSP13 (**Fig. 4C**), which was further validated by TEAD4 domain mapping (**fig. S4E**). Moreover, NSP13 interacted with the TEAD4 YAP binding domain, suggesting that the NSP13/TEAD4 interaction may disrupt the YAP/TEAD4 complex. Unexpectedly, NSP13 had no effect on the YAP/TEAD4 association, but the interaction between YAP and NSP13 was much stronger in the presence of TEAD4 than in its absence (**Fig. 4D**). These data collectively indicated that TEAD4 acts as a platform for recruiting YAP and NSP13, and that NSP13 conversely inactivates the YAP/TEAD4 complex (**Fig. 4E**). Moreover, NSP13 protein levels accumulated as YAP5SA expression in CMs (**Fig. 4F-G**), which supports the hypothesis that nuclear NSP13/YAP/TEAD4 prevents NSP13 from being degraded.

NSP13 recruits YAP endogenous suppressors into YAP/TEAD complex

Given that NSP13 interacted with YAP/TEAD4 complex but not disrupt YAP/TEAD4 interaction, we hypothesized that NSP13 recruits endogenous YAP suppressors to the YAP/TEAD4/NSP13 complex on DNA to inhibit YAP transactivation. To test this, we performed the IP-mass

spectrometry pulldown of NSP13 in HEK293T cell nuclei and analyzed NSP13-interacting proteins in the presence or absence of YAP expression. As shown in **Fig. 4H**, we obtained several candidate proteins that interact with NSP13 in the nucleus. Gene ontology analysis indicated that these genes regulate chromosome organization, the cell cycle, and protein folding (**fig. S4F**). We then tested the function of a select group of these proteins in YAP transactivation by performing siRNA knockdown studies in HEK293T cells, followed by a reporter assay for YAP transactivation. The siRNA knockdown efficiency for the YAP suppressors CCT3 and TTF2 is shown in **fig. S4G**. Reporter assay results revealed that the siRNA knockdown of CCT3 and TTF2 increased endogenous YAP transactivation in HEK293T cells (**Fig. 4I** and **fig. S4H**), suggesting that NSP13 suppressed YAP activity by recruiting these endogenous YAP suppressors to the YAP/TEAD4 complex.

DISCUSSION

Several years have passed since SARS-CoV-2 was identified as the virus responsible for the worldwide COVID-19 pandemic. Although COVID-19 vaccines help protect people from infection with SARS-CoV-2, and several promising anti-SARS-CoV-2 drugs have been developed, the long-term effect of COVID-19 and how SARS-CoV2 proteins affect the Hippo pathway remain largely unknown. Here, we reported that SARS-CoV-2 infection suppressed the activity of YAP, the downstream effector of Hippo signaling, in lung samples from patients with COVID-19 and in iPS-CMs. In addition, the screening of NSP proteins from SARS-CoV-2 indicated that NSP13 strongly inhibits YAP activity independent of Lats1/2 *in vitro*. By using a YAP5SA transgenic mouse model, we found that NSP13 reversed the heart failure phenotype in YAP5SA mice and increased the survival rate, supporting that NSP13 inhibits YAP5SA *in vivo*.

From a mechanistic standpoint, we found that NSP13 protein accumulated in the presence of high YAP activity and then suppressed YAP activity by recruiting its suppressors to the YAP/TEAD4/NSP13 complex.

The molecular mechanism of NSP13 suppression on YAP

NSP13 is a conserved coronavirus helicase and plays important roles in viral replication by cooperating with NSP7, NSP8, and NSP12 (*46-48*). Recent studies revealed that NSP13 suppressed interferon production by counteracting the antiviral signaling pathway (*18-21, 56, 57*). However, whether NSP13 affects other signaling pathways is unknown. Here, we showed that NSP13 suppressed YAP activity by recruiting YAP suppressors. Unexpectedly, however, NSP13 did not directly interact with YAP to restrain YAP in the cytoplasm, nor did it disrupt the YAP/TEAD4 interaction, despite that NSP13 and TEAD4 directly interact. Instead, NSP13 formed a complex with YAP/TEAD4 and recruited innate YAP suppressors. Several studies have shown that NSP13 is transiently expressed, primarily localizes in the cytoplasm of cells, and interacts with other proteins (*58-60*). By using the AAV9 virus, we expressed NSP13 in CMs and found that NSP13 localized in the nucleus and cytoplasm, suggesting that it may have a unique role *in vivo*. To uncover the mechanism for how NSP13 suppresses YAP, we performed IP-mass spectrometry screening in HEK293T cell nuclei to identify potential YAP suppressors. Several suppressors of YAP were identified, such as CCT3, CCT4, and TTF2. In addition, we found that NSP13 helicase activity marked by its ATP consumption and nucleic acid–binding ability is required for its suppression of YAP, suggesting that NSP13 may unwind DNA and anchor itself on the DNA to recruit TEAD4, which further recruits YAP suppressors to the YAP/TEAD4 complex.

SARS-CoV-2 infection in tissue with high YAP expression

Our data indicated that NSP13 protein accumulates in the presence of high YAP activity. We predicted that tissues with high YAP expression such as lung epithelium, intestine, liver, skin, and nervous system may face a greater threat than those with low YAP expression after infection with SARS-CoV-2, presumably because the increased NSP13 protein would strongly suppress YAP activity and disrupt tissue homeostasis. As shown in **Fig. 1B**, human lung epithelial cells were vulnerable to SARS-CoV-2 infection because the virus can directly attack AT1 and AT2 cells that highly express TMPRSS2. Covering more than 95% of the alveolar surface, AT1 cells were infected with SARS-CoV-2, which led to cell death or dysfunction because of low YAP activity. AT2 cells, which act as progenitor cells to regenerate AT1 and AT2 cell populations during repair, had unchanged YAP activity levels between control patients and patients with COVID-19. Therefore, we predicted that the lower YAP activity in AT2 cells infected with SARS-CoV-2 may decrease cell differentiation from AT2 cells to AT1 cells in lung samples from patients with COVID-19. Recent studies have shown that SARS-CoV-2 directly infects and replicates in patient intestinal epithelial cells (*61*), which is where YAP plays key roles in epithelial cell self-renewal, differentiation, and regeneration (*5, 62, 63*). Thus, the mechanism by which SARS-CoV-2 suppresses YAP may be partially responsible for the intestinal damage observed. Furthermore, these data suggest that the infection of tissues with SARS-CoV-2 that have high vs. low YAP activity or expression may have worse consequences. Clinical data related to COVID-19 and tissue regeneration are needed to further explore this mechanism.

NSP13 in innate immunity and beyond

YAP acts as the downstream effector of the Hippo signaling pathway by associating with transcription factors such as TEAD1-4 to activate the transcription of genes involved in cell proliferation. In addition to interacting with TEADs, YAP also interacts with and cooperates with other DNA-binding transcription factors, such as AP-1, SMAD, p73, and RUNX1/2, indicating a broad role for the Hippo pathway in physiology (*64*). Recently, emerging studies showed that the Hippo pathway also plays critical roles in innate immunity by directly interacting with the key components of innate immune response signaling or regulatory cytokines expression (*65, 66*). The non–cell autonomous effect of high YAP activity is important for the immune microenvironment. For example, high YAP activity in heart or liver resulted in the expansion of macrophages by inducing Ccl2 and Csf1 expression (*67, 68*). In this study, we reported that NSP13 suppressed YAP transactivation, suggesting that NSP13 inhibits innate immunity by regulating YAP. SARS-CoV-2 infection in host cells may reprogram the immune microenvironment including the suppression of YAP in macrophages.

Consistent with the importance of YAP as a transcriptional co-activator in regulating cell proliferation, YAP has been found to be hyperactive or highly expressed in cancers(*69*). In the presence of high YAP activity or expression, NSP13 introduction may strongly suppress the YAP/TEAD4–dependent expression of genes related to the cell cycle. On the other hand, NSP13 may reprogram the tumor microenvironment by orchestrating macrophage composition through the regulation of YAP. These two possibilities suggest NSP13 as a promising therapeutic in treating YAP-driven cancers.

In conclusion, our study reveals a novel function of NSP13 on YAP suppression and advances our understanding of the underlying effect of SARS-CoV-2 in host cells. These findings may also provide a new avenue for how to harness YAP activity as a potential treatment.

MATERIALS AND METHODS

Study design

The objective of this study was to explore how SARS-CoV-2 infection affects YAP, the downstream effector of Hippo signaling. We used RNA sequencing to analyze lung samples from patients infected with SARS-CoV-2 and iPSC-derived CMs. To determine which SARS-CoV-2 protein suppressed YAP transactivation, we used a dual-luciferase reporter assay system. Transgenic mice expressing constitutively active YAP (YAP5SA) were used for evaluating the effects of NSP13 suppression *in vivo*. Mouse survival rate, cardiac function, and tissue histology were examined. NSP13 mutant plasmids were studied to investigate whether the helicase activity of NSP13 is required for YAP suppression. To determine the mechanism for how NSP13 suppressed YAP activity, we used IF, IP-western blot, and IP-mass spectrometry analyses. We also used the Alpha-fold Protein structure database and performed siRNA experiments to support our working model. For all reporter assay experiments, a minimum of 3 measurements were recorded. The investigators were blinded to mouse groups when using echocardiography to record and analyze cardiac function. All western blot experiments involving the YAP/TEAD4/NSP13 complex in nuclei were performed at least three times.

RNA-seq analysis

For the analysis of lung samples from patients with COVID-19, data from 23 COVID-19 lung donor samples from GSE171668 (*36*) and 7 lung control donor samples from GSE171524 (*37*) were downloaded and analyzed using Seurat v4 software suite (*70*). A total of 143,470 cells were used in the analysis. Each sample was normalized and batch corrected using SCTransformation.

The mitochondrial percentage was used to regress out any technical variability between batches. Samples were integrated by using harmony (*71*) integration to remove technical variation. For the analysis of iPSC-derived CMs infected with SARS-CoV-2, bulk RNA-seq data was obtained from a study by Perez-Bermejo et al. (*44*). With this dataset, we re-analyzed and evaluated the average expression of 302 CM-specific YAP target genes (*45*).

Expression plasmids

Expression plasmids encoding HA-tagged wild-type, mutant, or truncated NSP13 were generated by PCR and subcloned into pXF4H (N-terminal HA tag) derived from pRK5 (Genetech). Myc-tagged wild-type or truncated TEAD4, flag-tagged wild-type YAP, and flag-tagged YAP5SA were generated by PCR and subcloned into a pcDNA3 backbone. HA-tagged wild-type Lats2, Lats2 KR, and pRL-TK_Luc were gifts from Dr. Pinglong Xu's lab. Reporters of HOP-flash (#83467) and 8xGTIIC-luciferase (#34615) were purchased from Addgene. The NSP plasmids used in YAP transactivation screening experiments were gifts from Dr. Nevan J. Krogan's lab. All plasmids were confirmed by performing DNA sequencing.

Cell culture and transfection

HEK293T and Hela cells were cultured in Dulbecco's Modified Eagle Medium with 10% fetal bovine serum (FBS). Lipofectamine™ 2000 (ThermoFisher) or Lipofectamine™ 3000 (ThermoFisher) reagents were used for plasmid transfection. LipofectAmine RNAiMAX (ThermoFisher) was used for siRNA transfection.

Luciferase reporter assay

HEK293T or Hela cells were transfected with wild-type YAP- or YAP5SA responsive HOP-flash plasmid or 8xGTIIC-luciferase reporter, which bears an open reading frame encoding firefly luciferase, along with the pRL-Luc with *Renilla* luciferase coding as the internal control for transfection and other expression vectors (NSPs), as specified. After 24 h of transfection with the indicated treatments, cells were lysed with passive lysis buffer (Promega). Luciferase assays were performed by using a dual-luciferase assay kit (Promega). Data were quantified with POLARstar Omega (BMG Labtech) and normalized to the internal *Renilla* luciferase control.

AAV9 viral packaging

Viral vectors were used as previously described (*72*). The construct containing HA-tagged NSP13 was cloned into the pENN.AAV.cTNT, p1967-Q vector (AAV9-HA-NSP13). Empty vector–encoding GFP was used as the control (AAV9-GFP). Both vectors were packaged into the muscle-trophic serotype AAV9 by the Intellectual and Developmental Disabilities Research Center Neuroconnectivity Core at the Baylor College of Medicine. After tittering, viruses were aliquoted (1×10^{13} viral genome particles per tube) and immediately frozen and placed at −80°C for long-term storage. Before each injection, each aliquot was diluted in saline to make a 120-ul injection solution.

Mice

For this study, the previously described mouse strains αMyHC-MerCreMer; WT mice and αMyHC-MerCreMer; YAP5SA mice were used(*45*). Mice had a mixed genetic background of C57BL/6 and 129SV. The AAV9 virus (a total of 5×10^{11} viral genomes, 120 µl total volume delivered) was delivered by retro-orbital injection 2 weeks before tamoxifen injection. Two doses

of tamoxifen (10 ug/g) were administered to mice that were 6 to weeks old by intraperitoneal injection.

Echocardiography

Cardiac function was analyzed by echocardiography. Imaging was performed on a VisualSonics Vevo 2100 system with a 550-s probe. B-mode images and M-mode images were captured on a short-axis projection. Ejection fraction, fractional shortening, diameter of diastolic left ventricle, diameter of systolic left ventricle, and end-diastolic volume were calculated by using a cardiac measurement package installed in the Vevo2100 system.

Histology and IF staining

For histology and IF staining, hearts were fixed in 4% paraformaldehyde overnight at 4 °C and dehydrated in serial ethanol and xylene solutions and embedded in paraffin. For IF staining, slides were sectioned at 10-um intervals. For paraffin sections, samples were deparaffinized and rehydrated, treated with 3% H_2O_2 in EtOH, treated with antigen retrieval solution (Vector Laboratories Inc., Burlingame, CA, USA), blocked with 10% donkey serum in phosphate-buffered saline, and then incubated with primary antibodies. The antibodies used rabbit anti-HA (#3724, Cell signaling) and rat anti-flag (NBP1-06712, Novus Bio-logicals). IF stained images were captured on a Zeiss LSM 780 NLO Confocal/2-hoton microscope.

References and Notes

1. S. Ma, Z. Meng, R. Chen, K. L. Guan, The Hippo pathway: Biology and pathophysiology. *Annu. Rev. Biochem.* **88**, 577-604 (2019).
2. J. Wang, S. Liu, T. Heallen, J. F. Martin, The Hippo pathway in the heart: pivotal roles in development, disease, and regeneration. *Nat. Rev. Cardiol* **15**, 672-684 (2018).
3. F. Meng, B. Xie, J. F. Martin, Targeting the Hippo pathway in heart repair. *Cardiovasc. Res.* **118**, 2402-2414 (2022).
4. J. O. Russell, F. D. Camargo, Hippo signalling in the liver: role in development, regeneration and disease. *Nat Rev Gastroenterol Hepatol* **19**, 297-312 (2022).
5. A. W. Hong, Z. Meng, K. L. Guan, The Hippo pathway in intestinal regeneration and disease. *Nat. Rev. Gastroenterol. Hepatol.* **13**, 324-337 (2016).
6. Y. Sun, D. Jin, Z. Zhang, D. Jin, J. Xue, L. Duan, Y. Zhang, X. Kang, F. Lian, The critical role of the Hippo signaling pathway in kidney diseases. *Front Pharmacol* **13**, 988175 (2022).
7. I. M. Moya, G. Halder, Hippo-YAP/TAZ signalling in organ regeneration and regenerative medicine. *Nat Rev Mol Cell Biol* **20**, 211-226 (2019).
8. Y. Zhang, H. Zhang, B. Zhao, Hippo signaling in the immune system. *Trends Biochem. Sci.* **43**, 77-80 (2018).
9. C. Ma, Y. Cong, H. Zhang, COVID-19 and the digestive system. *Am. J. Gastroenterol.* **115**, 1003-1006 (2020).
10. F. G. De Felice, F. Tovar-Moll, J. Moll, D. P. Munoz, S. T. Ferreira, Severe acute respiratory syndrome coronavirus 2 (SARS-CoV-2) and the central nervous system. *Trends Neurosci.* **43**, 355-357 (2020).
11. P. Gabarre, G. Dumas, T. Dupont, M. Darmon, E. Azoulay, L. Zafrani, Acute kidney injury in critically ill patients with COVID-19. *Intensive Care Med.* **46**, 1339-1348 (2020).
12. M. Nishiga, D. W. Wang, Y. Han, D. B. Lewis, J. C. Wu, COVID-19 and cardiovascular disease: from basic mechanisms to clinical perspectives. *Nat. Rev. Cardiol* **17**, 543-558 (2020).
13. J. Wu, Y. Shi, X. Pan, S. Wu, R. Hou, Y. Zhang, T. Zhong, H. Tang, W. Du, L. Wang, J. Wo, J. Mu, Y. Qiu, K. Yang, L. K. Zhang, B. C. Ye, N. Qi, SARS-CoV-2 ORF9b inhibits RIG-I-MAVS antiviral signaling by interrupting K63-linked ubiquitination of NEMO. *Cell Rep.* **34**, 108761 (2021).
14. G. Gori Savellini, G. Anichini, C. Gandolfo, M. G. Cusi, SARS-CoV-2 N protein targets TRIM25-mediated RIG-I activation to suppress innate immunity. *Viruses* **13**, (2021).
15. S. Wang, T. Dai, Z. Qin, T. Pan, F. Chu, L. Lou, L. Zhang, B. Yang, H. Huang, H. Lu, F. Zhou, Targeting liquid-liquid phase separation of SARS-CoV-2 nucleocapsid protein promotes innate antiviral immunity by elevating MAVS activity. *Nat. Cell Biol.* **23**, 718-732 (2021).
16. Y. Zhao, L. Sui, P. Wu, W. Wang, Z. Wang, Y. Yu, Z. Hou, G. Tan, Q. Liu, G. Wang, A dual-role of SARS-CoV-2 nucleocapsid protein in regulating innate immune response. *Signal Transduct. Target Ther.* **6**, 331 (2021).
17. J. C. Hsu, M. Laurent-Rolle, J. B. Pawlak, C. B. Wilen, P. Cresswell, Translational shutdown and evasion of the innate immune response by SARS-CoV-2 NSP14 protein. *Proc Natl Acad Sci U S A* **118**, (2021).

18. H. Xia, Z. Cao, X. Xie, X. Zhang, J. Y. Chen, H. Wang, V. D. Menachery, R. Rajsbaum, P. Y. Shi, Evasion of type I interferon by SARS-CoV-2. *Cell Rep.* **33**, 108234 (2020).
19. X. Lei, X. Dong, R. Ma, W. Wang, X. Xiao, Z. Tian, C. Wang, Y. Wang, L. Li, L. Ren, F. Guo, Z. Zhao, Z. Zhou, Z. Xiang, J. Wang, Activation and evasion of type I interferon responses by SARS-CoV-2. *Nat. Commun.* **11**, 3810 (2020).
20. G. Guo, M. Gao, X. Gao, B. Zhu, J. Huang, K. Luo, Y. Zhang, J. Sun, M. Deng, Z. Lou, SARS-CoV-2 non-structural protein 13 (nsp13) hijacks host deubiquitinase USP13 and counteracts host antiviral immune response. *Signal Transduct. Target Ther.* **6**, 119 (2021).
21. C. K. Yuen, J. Y. Lam, W. M. Wong, L. F. Mak, X. Wang, H. Chu, J. P. Cai, D. Y. Jin, K. K. To, J. F. Chan, K. Y. Yuen, K. H. Kok, SARS-CoV-2 nsp13, nsp14, nsp15 and orf6 function as potent interferon antagonists. *Emerg Microbes Infect* **9**, 1418-1428 (2020).
22. K. Feng, H. J. Zhang, Y. Q. Min, M. Zhou, F. Deng, H. L. Wang, P. Q. Li, Y. J. Ning, SARS-CoV-2 NSP13 interacts with host IRF3, blocking antiviral immune responses. *J. Med. Virol.* **95**, e28881 (2023).
23. D. E. Gordon, G. M. Jang, M. Bouhaddou, J. Xu, K. Obernier, K. M. White, M. J. O'Meara, V. V. Rezelj, J. Z. Guo, D. L. Swaney, T. A. Tummino, R. Huttenhain, R. M. Kaake, A. L. Richards, B. Tutuncuoglu, H. Foussard, J. Batra, K. Haas, M. Modak, M. Kim, P. Haas, B. J. Polacco, H. Braberg, J. M. Fabius, M. Eckhardt, M. Soucheray, M. J. Bennett, M. Cakir, M. J. McGregor, Q. Li, B. Meyer, F. Roesch, T. Vallet, A. Mac Kain, L. Miorin, E. Moreno, Z. Z. C. Naing, Y. Zhou, S. Peng, Y. Shi, Z. Zhang, W. Shen, I. T. Kirby, J. E. Melnyk, J. S. Chorba, K. Lou, S. A. Dai, I. Barrio-Hernandez, D. Memon, C. Hernandez-Armenta, J. Lyu, C. J. P. Mathy, T. Perica, K. B. Pilla, S. J. Ganesan, D. J. Saltzberg, R. Rakesh, X. Liu, S. B. Rosenthal, L. Calviello, S. Venkataramanan, J. Liboy-Lugo, Y. Lin, X. P. Huang, Y. Liu, S. A. Wankowicz, M. Bohn, M. Safari, F. S. Ugur, C. Koh, N. S. Savar, Q. D. Tran, D. Shengjuler, S. J. Fletcher, M. C. O'Neal, Y. Cai, J. C. J. Chang, D. J. Broadhurst, S. Klippsten, P. P. Sharp, N. A. Wenzell, D. Kuzuoglu-Ozturk, H. Y. Wang, R. Trenker, J. M. Young, D. A. Cavero, J. Hiatt, T. L. Roth, U. Rathore, A. Subramanian, J. Noack, M. Hubert, R. M. Stroud, A. D. Frankel, O. S. Rosenberg, K. A. Verba, D. A. Agard, M. Ott, M. Emerman, N. Jura, M. von Zastrow, E. Verdin, A. Ashworth, O. Schwartz, C. d'Enfert, S. Mukherjee, M. Jacobson, H. S. Malik, D. G. Fujimori, T. Ideker, C. S. Craik, S. N. Floor, J. S. Fraser, J. D. Gross, A. Sali, B. L. Roth, D. Ruggero, J. Taunton, T. Kortemme, P. Beltrao, M. Vignuzzi, A. Garcia-Sastre, K. M. Shokat, B. K. Shoichet, N. J. Krogan, A SARS-CoV-2 protein interaction map reveals targets for drug repurposing. *Nature* **583**, 459-468 (2020).
24. P. V'Kovski, A. Kratzel, S. Steiner, H. Stalder, V. Thiel, Coronavirus biology and replication: implications for SARS-CoV-2. *Nat Rev Microbiol* **19**, 155-170 (2021).
25. R. Terracciano, M. Preiano, A. Fregola, C. Pelaia, T. Montalcini, R. Savino, Mapping the SARS-CoV-2-host protein-protein interactome by affinity purification mass spectrometry and proximity-dependent biotin labeling: a rational and straightforward route to discover host-directed anti-SARS-CoV-2 therapeutics. *Int. J. Mol. Sci.* **22**, (2021).
26. D. E. Gordon, J. Hiatt, M. Bouhaddou, V. V. Rezelj, S. Ulferts, H. Braberg, A. S. Jureka, K. Obernier, J. Z. Guo, J. Batra, R. M. Kaake, A. R. Weckstein, T. W. Owens, M. Gupta, S. Pourmal, E. W. Titus, M. Cakir, M. Soucheray, M. McGregor, Z. Cakir, G. Jang, M. J. O'Meara, T. A. Tummino, Z. Zhang, H. Foussard, A. Rojc, Y. Zhou, D. Kuchenov, R. Huttenhain, J. Xu, M. Eckhardt, D. L. Swaney, J. M. Fabius, M. Ummadi, B. Tutuncuoglu, U. Rathore, M. Modak, P. Haas, K. M. Haas, Z. Z. C. Naing, E. H. Pulido, Y. Shi, I. Barrio-

Hernandez, D. Memon, E. Petsalaki, A. Dunham, M. C. Marrero, D. Burke, C. Koh, T. Vallet, J. A. Silvas, C. M. Azumaya, C. Billesbolle, A. F. Brilot, M. G. Campbell, A. Diallo, M. S. Dickinson, D. Diwanji, N. Herrera, N. Hoppe, H. T. Kratochvil, Y. Liu, G. E. Merz, M. Moritz, H. C. Nguyen, C. Nowotny, C. Puchades, A. N. Rizo, U. Schulze-Gahmen, A. M. Smith, M. Sun, I. D. Young, J. Zhao, D. Asarnow, J. Biel, A. Bowen, J. R. Braxton, J. Chen, C. M. Chio, U. S. Chio, I. Deshpande, L. Doan, B. Faust, S. Flores, M. Jin, K. Kim, V. L. Lam, F. Li, J. Li, Y. L. Li, Y. Li, X. Liu, M. Lo, K. E. Lopez, A. A. Melo, F. R. Moss, 3rd, P. Nguyen, J. Paulino, K. I. Pawar, J. K. Peters, T. H. Pospiech, Jr., M. Safari, S. Sangwan, K. Schaefer, P. V. Thomas, A. C. Thwin, R. Trenker, E. Tse, T. K. M. Tsui, F. Wang, N. Whitis, Z. Yu, K. Zhang, Y. Zhang, F. Zhou, D. Saltzberg, Q. S. B. Consortium, A. J. Hodder, A. S. Shun-Shion, D. M. Williams, K. M. White, R. Rosales, T. Kehrer, L. Miorin, E. Moreno, A. H. Patel, S. Rihn, M. M. Khalid, A. Vallejo-Gracia, P. Fozouni, C. R. Simoneau, T. L. Roth, D. Wu, M. A. Karim, M. Ghoussaini, I. Dunham, F. Berardi, S. Weigang, M. Chazal, J. Park, J. Logue, M. McGrath, S. Weston, R. Haupt, C. J. Hastie, M. Elliott, F. Brown, K. A. Burness, E. Reid, M. Dorward, C. Johnson, S. G. Wilkinson, A. Geyer, D. M. Giesel, C. Baillie, S. Raggett, H. Leech, R. Toth, N. Goodman, K. C. Keough, A. L. Lind, C. Zoonomia, R. J. Klesh, K. R. Hemphill, J. Carlson-Stevermer, J. Oki, K. Holden, T. Maures, K. S. Pollard, A. Sali, D. A. Agard, Y. Cheng, J. S. Fraser, A. Frost, N. Jura, T. Kortemme, A. Manglik, D. R. Southworth, R. M. Stroud, D. R. Alessi, P. Davies, M. B. Frieman, T. Ideker, C. Abate, N. Jouvenet, G. Kochs, B. Shoichet, M. Ott, M. Palmarini, K. M. Shokat, A. Garcia-Sastre, J. A. Rassen, R. Grosse, O. S. Rosenberg, K. A. Verba, C. F. Basler, M. Vignuzzi, A. A. Peden, P. Beltrao, N. J. Krogan, Comparative host-coronavirus protein interaction networks reveal pan-viral disease mechanisms. *Science* **370**, (2020).

27. J. P. Davies, K. M. Almasy, E. F. McDonald, L. Plate, Comparative multiplexed interactomics of SARS-CoV-2 and homologous coronavirus nonstructural proteins identifies unique and shared host-cell dependencies. *ACS Infect Dis* **6**, 3174-3189 (2020).
28. Z. Chen, C. Wang, X. Feng, L. Nie, M. Tang, H. Zhang, Y. Xiong, S. K. Swisher, M. Srivastava, J. Chen, Interactomes of SARS-CoV-2 and human coronaviruses reveal host factors potentially affecting pathogenesis. *EMBO J.* **40**, e107776 (2021).
29. A. Stukalov, V. Girault, V. Grass, O. Karayel, V. Bergant, C. Urban, D. A. Haas, Y. Huang, L. Oubraham, A. Wang, M. S. Hamad, A. Piras, F. M. Hansen, M. C. Tanzer, I. Paron, L. Zinzula, T. Engleitner, M. Reinecke, T. M. Lavacca, R. Ehmann, R. Wolfel, J. Jores, B. Kuster, U. Protzer, R. Rad, J. Ziebuhr, V. Thiel, P. Scaturro, M. Mann, A. Pichlmair, Multilevel proteomics reveals host perturbations by SARS-CoV-2 and SARS-CoV. *Nature* **594**, 246-252 (2021).
30. D. G. May, L. Martin-Sancho, V. Anschau, S. Liu, R. J. Chrisopulos, K. L. Scott, C. T. Halfmann, R. D. Pena, D. Pratt, A. R. Campos, K. J. Roux, A BioID-derived proximity interactome for SARS-CoV-2 proteins. *bioRxiv*, (2021).
31. Y. Zhang, L. Shang, J. Zhang, Y. Liu, C. Jin, Y. Zhao, X. Lei, W. Wang, X. Xiao, X. Zhang, Y. Liu, L. Liu, M. W. Zhuang, Q. Mi, C. Tian, J. Wang, F. He, P. H. Wang, J. Wang, An antibody-based proximity labeling map reveals mechanisms of SARS-CoV-2 inhibition of antiviral immunity. *Cell Chem Biol*, (2021).
32. E. M. N. Laurent, Y. Sofianatos, A. Komarova, J.-P. Gimeno, P. S. Tehrani, D.-K. Kim, H. Abdouni, M. Duhamel, P. Cassonnet, J. J. Knapp, D. Kuang, A. Chawla, D. Sheykhkarimli, A. Rayhan, R. Li, O. Pogoutse, D. E. Hill, M. A. Calderwood, P. Falter-

Braun, P. Aloy, U. Stelzl, M. Vidal, A.-C. Gingras, G. A. Pavlopoulos, S. Van Der Werf, I. Fournier, F. P. Roth, M. Salzet, C. Demeret, Y. Jacob, E. Coyaud, Global BioID-based SARS-CoV-2 proteins proximal interactome unveils novel ties between viral polypeptides and host factors involved in multiple COVID19-associated mechanisms. *bioRxiv*, 2020.2008.2028.272955 (2020).

33. P. Samavarchi-Tehrani, H. Abdouni, J. D. R. Knight, A. Astori, R. Samson, Z.-Y. Lin, D.-K. Kim, J. J. Knapp, J. St-Germain, C. D. Go, B. Larsen, C. J. Wong, P. Cassonnet, C. Demeret, Y. Jacob, F. P. Roth, B. Raught, A.-C. Gingras, A SARS-CoV-2 – host proximity interactome. *bioRxiv*, 2020.2009.2003.282103 (2020).
34. J. R. St-Germain, A. Astori, P. Samavarchi-Tehrani, H. Abdouni, V. Macwan, D.-K. Kim, J. J. Knapp, F. P. Roth, A.-C. Gingras, B. Raught, A SARS-CoV-2 BioID-based virus-host membrane protein interactome and virus peptide compendium: new proteomics resources for COVID-19 research. *bioRxiv*, 2020.2008.2028.269175 (2020).
35. D.-K. Kim, B. Weller, C.-W. Lin, D. Sheykhkarimli, J. J. Knapp, N. Kishore, M. Sauer, A. Rayhan, V. Young, N. Marin-de la Rosa, O. Pogoutse, K. Spirohn, A. Strobel, F. Laval, P. Schwehn, R. Li, S. Rothballer, M. Altmann, P. Cassonnet, G. Dugied, A. G. Cote, L. E. Vergara, I. Hazelwood, B. B. Liu, M. Nguyen, R. Pandiarajan, P. A. Rodriguez Coloma, L. Willems, J.-C. Twizere, C. Demeret, Y. Jacob, T. Hao, D. E. Hill, C. Falter, M. Vidal, M. A. Calderwood, F. P. Roth, P. Falter-Braun, A map of binary SARS-CoV-2 protein interactions implicates host immune regulation and ubiquitination. *bioRxiv*, 2021.2003.2015.433877 (2021).
36. T. M. Delorey, C. G. K. Ziegler, G. Heimberg, R. Normand, Y. Yang, A. Segerstolpe, D. Abbondanza, S. J. Fleming, A. Subramanian, D. T. Montoro, K. A. Jagadeesh, K. K. Dey, P. Sen, M. Slyper, Y. H. Pita-Juarez, D. Phillips, J. Biermann, Z. Bloom-Ackermann, N. Barkas, A. Ganna, J. Gomez, J. C. Melms, I. Katsyv, E. Normandin, P. Naderi, Y. V. Popov, S. S. Raju, S. Niezen, L. T. Tsai, K. J. Siddle, M. Sud, V. M. Tran, S. K. Vellarikkal, Y. Wang, L. Amir-Zilberstein, D. S. Atri, J. Beechem, O. R. Brook, J. Chen, P. Divakar, P. Dorceus, J. M. Engreitz, A. Essene, D. M. Fitzgerald, R. Fropf, S. Gazal, J. Gould, J. Grzyb, T. Harvey, J. Hecht, T. Hether, J. Jane-Valbuena, M. Leney-Greene, H. Ma, C. McCabe, D. E. McLoughlin, E. M. Miller, C. Muus, M. Niemi, R. Padera, L. Pan, D. Pant, C. Pe'er, J. Pfiffner-Borges, C. J. Pinto, J. Plaisted, J. Reeves, M. Ross, M. Rudy, E. H. Rueckert, M. Siciliano, A. Sturm, E. Todres, A. Waghray, S. Warren, S. Zhang, D. R. Zollinger, L. Cosimi, R. M. Gupta, N. Hacohen, H. Hibshoosh, W. Hide, A. L. Price, J. Rajagopal, P. R. Tata, S. Riedel, G. Szabo, T. L. Tickle, P. T. Ellinor, D. Hung, P. C. Sabeti, R. Novak, R. Rogers, D. E. Ingber, Z. G. Jiang, D. Juric, M. Babadi, S. L. Farhi, B. Izar, J. R. Stone, I. S. Vlachos, I. H. Solomon, O. Ashenberg, C. B. M. Porter, B. Li, A. K. Shalek, A. C. Villani, O. Rozenblatt-Rosen, A. Regev, COVID-19 tissue atlases reveal SARS-CoV-2 pathology and cellular targets. *Nature* **595**, 107-113 (2021).
37. J. C. Melms, J. Biermann, H. Huang, Y. Wang, A. Nair, S. Tagore, I. Katsyv, A. F. Rendeiro, A. D. Amin, D. Schapiro, C. J. Frangieh, A. M. Luoma, A. Filliol, Y. Fang, H. Ravichandran, M. G. Clausi, G. A. Alba, M. Rogava, S. W. Chen, P. Ho, D. T. Montoro, A. E. Kornberg, A. S. Han, M. F. Bakhoum, N. Anandasabapathy, M. Suarez-Farinas, S. F. Bakhoum, Y. Bram, A. Borczuk, X. V. Guo, J. H. Lefkowitch, C. Marboe, S. M. Lagana, A. Del Portillo, E. J. Tsai, E. Zorn, G. S. Markowitz, R. F. Schwabe, R. E. Schwartz, O. Elemento, A. Saqi, H. Hibshoosh, J. Que, B. Izar, A molecular single-cell lung atlas of lethal COVID-19. *Nature* **595**, 114-119 (2021).

38. M. Hoffmann, H. Kleine-Weber, S. Schroeder, N. Kruger, T. Herrler, S. Erichsen, T. S. Schiergens, G. Herrler, N. H. Wu, A. Nitsche, M. A. Muller, C. Drosten, S. Pohlmann, SARS-CoV-2 Cell Entry Depends on ACE2 and TMPRSS2 and Is Blocked by a Clinically Proven Protease Inhibitor. *Cell* **181**, 271-280 e278 (2020).
39. J. Koch, Z. M. Uckeley, P. Doldan, M. Stanifer, S. Boulant, P. Y. Lozach, TMPRSS2 expression dictates the entry route used by SARS-CoV-2 to infect host cells. *EMBO J* **40**, e107821 (2021).
40. R. Zang, M. F. Gomez Castro, B. T. McCune, Q. Zeng, P. W. Rothlauf, N. M. Sonnek, Z. Liu, K. F. Brulois, X. Wang, H. B. Greenberg, M. S. Diamond, M. A. Ciorba, S. P. J. Whelan, S. Ding, TMPRSS2 and TMPRSS4 promote SARS-CoV-2 infection of human small intestinal enterocytes. *Sci. Immunol.* **5**, (2020).
41. M. M. Lamers, B. L. Haagmans, SARS-CoV-2 pathogenesis. *Nat Rev Microbiol* **20**, 270-284 (2022).
42. I. J. Penkala, D. C. Liberti, J. Pankin, A. Sivakumar, M. M. Kremp, S. Jayachandran, J. Katzen, J. P. Leach, R. Windmueller, K. Stolz, M. P. Morley, A. Babu, S. Zhou, D. B. Frank, E. E. Morrisey, Age-dependent alveolar epithelial plasticity orchestrates lung homeostasis and regeneration. *Cell Stem Cell* **28**, 1775-1789 e1775 (2021).
43. J. J. Gokey, J. Snowball, A. Sridharan, P. Sudha, J. A. Kitzmiller, Y. Xu, J. A. Whitsett, YAP regulates alveolar epithelial cell differentiation and AGER via NFIB/KLF5/NKX2-1. *iScience* **24**, 102967 (2021).
44. J. A. Perez-Bermejo, S. Kang, S. J. Rockwood, C. R. Simoneau, D. A. Joy, A. C. Silva, G. N. Ramadoss, W. R. Flanigan, P. Fozouni, H. Li, P. Y. Chen, K. Nakamura, J. D. Whitman, P. J. Hanson, B. M. McManus, M. Ott, B. R. Conklin, T. C. McDevitt, SARS-CoV-2 infection of human iPSC-derived cardiac cells reflects cytopathic features in hearts of patients with COVID-19. *Sci. Transl. Med.* **13**, (2021).
45. T. O. Monroe, M. C. Hill, Y. Morikawa, J. P. Leach, T. Heallen, S. Cao, P. H. L. Krijger, W. de Laat, X. H. T. Wehrens, G. G. Rodney, J. F. Martin, YAP partially reprograms chromatin accessibility to directly induce adult cardiogenesis in vivo. *Dev. Cell* **48**, 765-779 e767 (2019).
46. L. Yan, J. Ge, L. Zheng, Y. Zhang, Y. Gao, T. Wang, Y. Huang, Y. Yang, S. Gao, M. Li, Z. Liu, H. Wang, Y. Li, Y. Chen, L. W. Guddat, Q. Wang, Z. Rao, Z. Lou, Cryo-EM structure of an extended SARS-CoV-2 replication and transcription complex reveals an intermediate state in cap synthesis. *Cell* **184**, 184-193 e110 (2021).
47. J. Chen, B. Malone, E. Llewellyn, M. Grasso, P. M. M. Shelton, P. D. B. Olinares, K. Maruthi, E. T. Eng, H. Vatandaslar, B. T. Chait, T. M. Kapoor, S. A. Darst, E. A. Campbell, Structural basis for helicase-polymerase coupling in the SARS-CoV-2 replication-transcription complex. *Cell* **182**, 1560-1573 e1513 (2020).
48. L. Yan, Y. Zhang, J. Ge, L. Zheng, Y. Gao, T. Wang, Z. Jia, H. Wang, Y. Huang, M. Li, Q. Wang, Z. Rao, Z. Lou, Architecture of a SARS-CoV-2 mini replication and transcription complex. *Nat. Commun.* **11**, 5874 (2020).
49. J. A. Newman, A. Douangamath, S. Yadzani, Y. Yosaatmadja, A. Aimon, J. Brandao-Neto, L. Dunnett, T. Gorrie-Stone, R. Skyner, D. Fearon, M. Schapira, F. von Delft, O. Gileadi, Structure, mechanism and crystallographic fragment screening of the SARS-CoV-2 NSP13 helicase. *Nat. Commun.* **12**, 4848 (2021).
50. J. Chen, Q. Wang, B. Malone, E. Llewellyn, Y. Pechersky, K. Maruthi, E. T. Eng, J. K. Perry, E. A. Campbell, D. E. Shaw, S. A. Darst, Ensemble cryo-EM reveals conformational

states of the nsp13 helicase in the SARS-CoV-2 helicase replication-transcription complex. *Nat Struct Mol Biol* **29**, 250-260 (2022).

51. B. Malone, J. Chen, Q. Wang, E. Llewellyn, Y. J. Choi, P. D. B. Olinares, X. Cao, C. Hernandez, E. T. Eng, B. T. Chait, D. E. Shaw, R. Landick, S. A. Darst, E. A. Campbell, Structural basis for backtracking by the SARS-CoV-2 replication-transcription complex. *Proc Natl Acad Sci U S A* **118**, (2021).
52. R. Nandi, D. Bhowmik, R. Srivastava, A. Prakash, D. Kumar, Discovering potential inhibitors against SARS-CoV-2 by targeting Nsp13 Helicase. *J. Biomol. Struct. Dyn.* **40**, 12062-12074 (2022).
53. J. Zeng, F. Weissmann, A. P. Bertolin, V. Posse, B. Canal, R. Ulferts, M. Wu, R. Harvey, S. Hussain, J. C. Milligan, C. Roustan, A. Borg, L. McCoy, L. S. Drury, S. Kjaer, J. McCauley, M. Howell, R. Beale, J. F. X. Diffley, Identifying SARS-CoV-2 antiviral compounds by screening for small molecule inhibitors of nsp13 helicase. *Biochem. J.* **478**, 2405-2423 (2021).
54. B. Zhao, X. Wei, W. Li, R. S. Udan, Q. Yang, J. Kim, J. Xie, T. Ikenoue, J. Yu, L. Li, P. Zheng, K. Ye, A. Chinnaiyan, G. Halder, Z. C. Lai, K. L. Guan, Inactivation of YAP oncoprotein by the Hippo pathway is involved in cell contact inhibition and tissue growth control. *Genes Dev* **21**, 2747-2761 (2007).
55. Z. Jia, L. Yan, Z. Ren, L. Wu, J. Wang, J. Guo, L. Zheng, Z. Ming, L. Zhang, Z. Lou, Z. Rao, Delicate structural coordination of the Severe Acute Respiratory Syndrome coronavirus Nsp13 upon ATP hydrolysis. *Nucleic Acids Res.* **47**, 6538-6550 (2019).
56. K. Feng, Y. Q. Min, X. Sun, F. Deng, P. Li, H. Wang, Y. J. Ning, Interactome profiling reveals interaction of SARS-CoV-2 NSP13 with host factor STAT1 to suppress interferon signaling. *J Mol Cell Biol*, (2021).
57. C. Vazquez, S. E. Swanson, S. G. Negatu, M. Dittmar, J. Miller, H. R. Ramage, S. Cherry, K. A. Jurado, SARS-CoV-2 viral proteins NSP1 and NSP13 inhibit interferon activation through distinct mechanisms. *PLoS One* **16**, e0253089 (2021).
58. J. Zhang, R. Cruz-Cosme, M. W. Zhuang, D. Liu, Y. Liu, S. Teng, P. H. Wang, Q. Tang, A systemic and molecular study of subcellular localization of SARS-CoV-2 proteins. *Signal Transduct Target Ther* **5**, 269 (2020).
59. X. Liu, S. Huuskonen, T. Laitinen, T. Redchuk, M. Bogacheva, K. Salokas, I. Pohner, T. Ohman, A. K. Tonduru, A. Hassinen, L. Gawriyski, S. Keskitalo, M. K. Vartiainen, V. Pietiainen, A. Poso, M. Varjosalo, SARS-CoV-2-host proteome interactions for antiviral drug discovery. *Mol Syst Biol* **17**, e10396 (2021).
60. F. S. Shi, Y. Yu, Y. L. Li, L. Cui, Z. Zhao, M. Wang, B. Wang, R. Zhang, Y. W. Huang, Expression Profile and Localization of SARS-CoV-2 Nonstructural Replicase Proteins in Infected Cells. *Microbiol Spectr* **10**, e0074422 (2022).
61. X. Wu, H. Jing, C. Wang, Y. Wang, N. Zuo, T. Jiang, V. A. Novakovic, J. Shi, Intestinal Damage in COVID-19: SARS-CoV-2 Infection and Intestinal Thrombosis. *Front Microbiol* **13**, 860931 (2022).
62. S. Fallah, J. F. Beaulieu, The Hippo Pathway Effector YAP1 Regulates Intestinal Epithelial Cell Differentiation. *Cells* **9**, (2020).
63. F. Deng, Z. Wu, F. Zou, S. Wang, X. Wang, The Hippo-YAP/TAZ Signaling Pathway in Intestinal Self-Renewal and Regeneration After Injury. *Front Cell Dev Biol* **10**, 894737 (2022).

64. F. Meng, B. Xie, J. F. Martin, Targeting the Hippo pathway in heart repair. *Cardiovasc Res*, (2021).
65. Q. Zhang, R. Zhou, P. Xu, The Hippo pathway in innate anti-microbial immunity and anti-tumor immunity. *Front. Immunol.* **11**, 1473 (2020).
66. S. Wang, L. Zhou, L. Ling, X. Meng, F. Chu, S. Zhang, F. Zhou, The crosstalk between Hippo-YAP pathway and innate immunity. *Front. Immunol.* **11**, 323 (2020).
67. Y. Xiao, M. C. Hill, L. Li, V. Deshmukh, T. J. Martin, J. Wang, J. F. Martin, Hippo pathway deletion in adult resting cardiac fibroblasts initiates a cell state transition with spontaneous and self-sustaining fibrosis. *Genes Dev.* **33**, 1491-1505 (2019).
68. X. Guo, Y. Zhao, H. Yan, Y. Yang, S. Shen, X. Dai, X. Ji, F. Ji, X. G. Gong, L. Li, X. Bai, X. H. Feng, T. Liang, J. Ji, L. Chen, H. Wang, B. Zhao, Single tumor-initiating cells evade immune clearance by recruiting type II macrophages. *Genes Dev* **31**, 247-259 (2017).
69. J. M. Franklin, Z. Wu, K. L. Guan, Insights into recent findings and clinical application of YAP and TAZ in cancer. *Nat Rev Cancer* **23**, 512-525 (2023).
70. Y. Hao, S. Hao, E. Andersen-Nissen, W. M. Mauck, 3rd, S. Zheng, A. Butler, M. J. Lee, A. J. Wilk, C. Darby, M. Zager, P. Hoffman, M. Stoeckius, E. Papalexi, E. P. Mimitou, J. Jain, A. Srivastava, T. Stuart, L. M. Fleming, B. Yeung, A. J. Rogers, J. M. McElrath, C. A. Blish, R. Gottardo, P. Smibert, R. Satija, Integrated analysis of multimodal single-cell data. *Cell* **184**, 3573-3587 e3529 (2021).
71. I. Korsunsky, N. Millard, J. Fan, K. Slowikowski, F. Zhang, K. Wei, Y. Baglaenko, M. Brenner, P. R. Loh, S. Raychaudhuri, Fast, sensitive and accurate integration of single-cell data with Harmony. *Nat Methods* **16**, 1289-1296 (2019).
72. J. P. Leach, T. Heallen, M. Zhang, M. Rahmani, Y. Morikawa, M. C. Hill, A. Segura, J. T. Willerson, J. F. Martin, Hippo pathway deficiency reverses systolic heart failure after infarction. *Nature* **550**, 260-264 (2017).

Competing interest statement

J.F.M is a founder and owns shares in Yap therapeutics. J.F.M. is a co-inventor on the following patents associated with this study: patent no. US20200206327A1 entitled "Hippo pathway deficiency reverses systolic heart failure post-infarction," patent no.15/642200.PCT/US2014/069349 101191411 entitled "Hippo and dystrophin complex signaling in cardiomyocyte renewal," and patent no. 15/102593.PCT/US2014/069349 9732345 entitled "Hippo and dystrophin complex signaling in cardiomyocyte renewal."

Acknowledgments

We are grateful to Drs. Nevan J. Krogan and Pinglong Xu for the gift of plasmids. Dr. Hongxin Guan helped with NSP13 mutant structure analysis. Nicole Stancel, PhD, ELS(D), of Scientific Publications at The Texas Heart Institute, provided editorial support.

Author contributions

Conceptualization: FM, JFM

Methodology: JK, XL, JS

Investigation: FM, C-RT, JW, YS, VD, BX, RL

Supervision: JFM

Writing – original draft: FM

Writing – review & editing: FM, JFM

Figure Legends

Fig. 1. Suppression of YAP activity by SARS-CoV-2 infection in vivo and in vitro. (**A**) UMAP of cell types in total lung snRNA-seq data. (**B**) UMAP visualization of TMPRESS2 expression in all cell types. (**C**) (Left) Subset clustering of epithelial cells labeled as AT1 and AT2. (Right) Violin plot of TMPRESS2 expression in AT1 and AT2 epithelial cells. (**D**) Comparison of Yap activity measured in AT1 and AT2 epithelial cells between Covid vs. control samples. *t*-test p-values: ***p < 0.001. (**E**) Box plot showing the mean expression scores of known YAP target genes in iPSC-CM bulk RNA-seq data. Each dot represents a biological replicate. The bottom and top of the box represent the lower (Q1) and upper (Q3) quartiles, respectively. The horizontal line inside the box indicates the median (Q2). The whiskers extend to the minimum and maximum values within 1.5 times the interquartile range (IQR) from the lower and upper quartiles, respectively. *t*-test p-values: **p < 0.01, ****p < 0.0001. (**F**) Heatmap displaying the expression Z-scores of example YAP targets in the iPSC-CM bulk RNA-seq data. Each column corresponds to a single biological sample.

Fig. 2. Inhibition of YAP in vitro and in vivo. (**A**) Results of screening NSPs for YAP activation using a reporter assay (Hopflash). Compared with other NSPs, NSP13 strongly inhibited YAP transactivation at low levels of protein expression. n = 3 independent experiments (mean ± SD). **** p < 0.0001, determined by using ANOVA and the Bonferroni correction. (**B**) Reporter assay (8*GTIIC) results showing that NSP13 but not YAP upstream kinase Lats2 inhibits YAP5SA transactivation in a dose-dependent manner. n = 3 independent experiments (mean ± SD). ***p < 0.001, **** p < 0.0001, determined by using ANOVA and the Bonferroni correction. (**C**) NSP13 expression at different time

points in mouse hearts after AAV9-HA-NSP13 virus injection. (**D**) Experimental design of studies in mice. (**E**) NSP13 expression in CMs rescued survival in YAP5SA mice after TAM injection. **p=0.0099, determined by using the log-rank test. (**F**) EF in YAP5SA mice was increased on day 8 and 14 after TAM injection (10 ug/g*2) and was reverted by NSP13 expression. *$p < 0.05$, ****$p < 0.001$, determined by using ANOVA and the Bonferroni correction. (**G**) Representative B-mode and M-mode echocardiographic images of the four groups of mice 8 days after TAM induction. (**H**) The smaller left ventricle chamber, as evidenced by the diameter of the diastolic left ventricle, in YAP5SA mice was rescued by NSP13 introduction. **$p < 0.01$, determined by using ANOVA and the Bonferroni correction. (**I-J**) Representative whole mount and H&E images of mouse hearts at 21 days after TAM induction. Scale bar, 2 mm.

Fig. 3. Requirement of NSP13 helicase activity for suppressing YAP activity. (**A**) Conserved amino acid sequences of NSP13 among Bat/pangolin SARS-CoVs. (**B**) Reporter assay results indicating that NSP13-R567A, which loses its ATP consumption ability, did not inhibit YAP5SA transactivation, whereas NSP13 K345A/K347A, which loses its nucleic acid binding activity, mildly promoted YAP5SA transactivation. n = 3 independent experiments (mean ± SD). **$p < 0.01$, **** $p < 0.0001$, determined by using ANOVA and the Bonferroni correction. (**C**) Map showing NSP13 domains. (**D**) Reporter assay results indicating that NSP13 truncations did not inhibit YAP 5SA transactivation, whereas the NSP13 DNA binding domains 1A and 2A slightly increased YAP5SA activation. n = 3 independent experiments (mean ± SD). *$p < 0.05$, **** $p < 0.0001$, determined by using ANOVA and the Bonferroni correction. (**E**) NSP13 mutants from SARS-CoV2 variants are shown. (**F**) Reporter assay (Hopflash) results indicating that NSP13 mutations did not

affect its suppression of YAP5SA transactivation. **** $p < 0.0001$, determined by using ANOVA and the Bonferroni correction.

Fig. 4. NSP13 inactivates YAP/TEAD4 complex by recruiting YAP suppressors. (**A**) Immunofluorescence imaging showing that NSP13 colocalized with YAP5SA in the cardiomyocytes of YAP5SA transgenic mice at 3 days after TAM injection. (**B**) Co-immunoprecipitation results suggesting that NSP13 interacts with TEAD4 in the nucleus. (**C**) The Alfa-fold prediction of the TEAD4/NSP13 interaction indicating that both the N- and C-terminal ends of TEAD4 are required for NSP13 interaction. TEAD4 interacted with NSP13 via its YAP binding domain (YBD). (**D**) Results of co-immunoprecipitation experiments in nuclei showing that NSP13 did not disrupt the interaction between YAP and TEAD4, whereas TEAD4 promoted the interaction between YAP and NSP13. (**E**) A working model for the YAP/TEAD4/NSP13 complex. TEAD4 acts as a platform for recruiting YAP and NSP13. (**F-G**) Immunofluorescence imaging and Western blot analysis showing that NSP13 protein levels increased in presence of high YAP expression. (**H**) Immunoprecipitation (IP)-MS in nuclei (IP: NSP13) suggesting NSP13 interacting proteins with or without YAP co-expression. (**I**) Reporter assay (Hopflash) results from Hela cells revealing that endogenous YAP activity was elevated after the siRNA-mediated knockdown of CCT3, CCT4, and TTF2. * $p < 0.05$, ** $p < 0.01$, determined by using ANOVA and the Bonferroni correction.

Figure 1. SARS-CoV-2 infection suppresses YAP activity in vivo and in vitro.

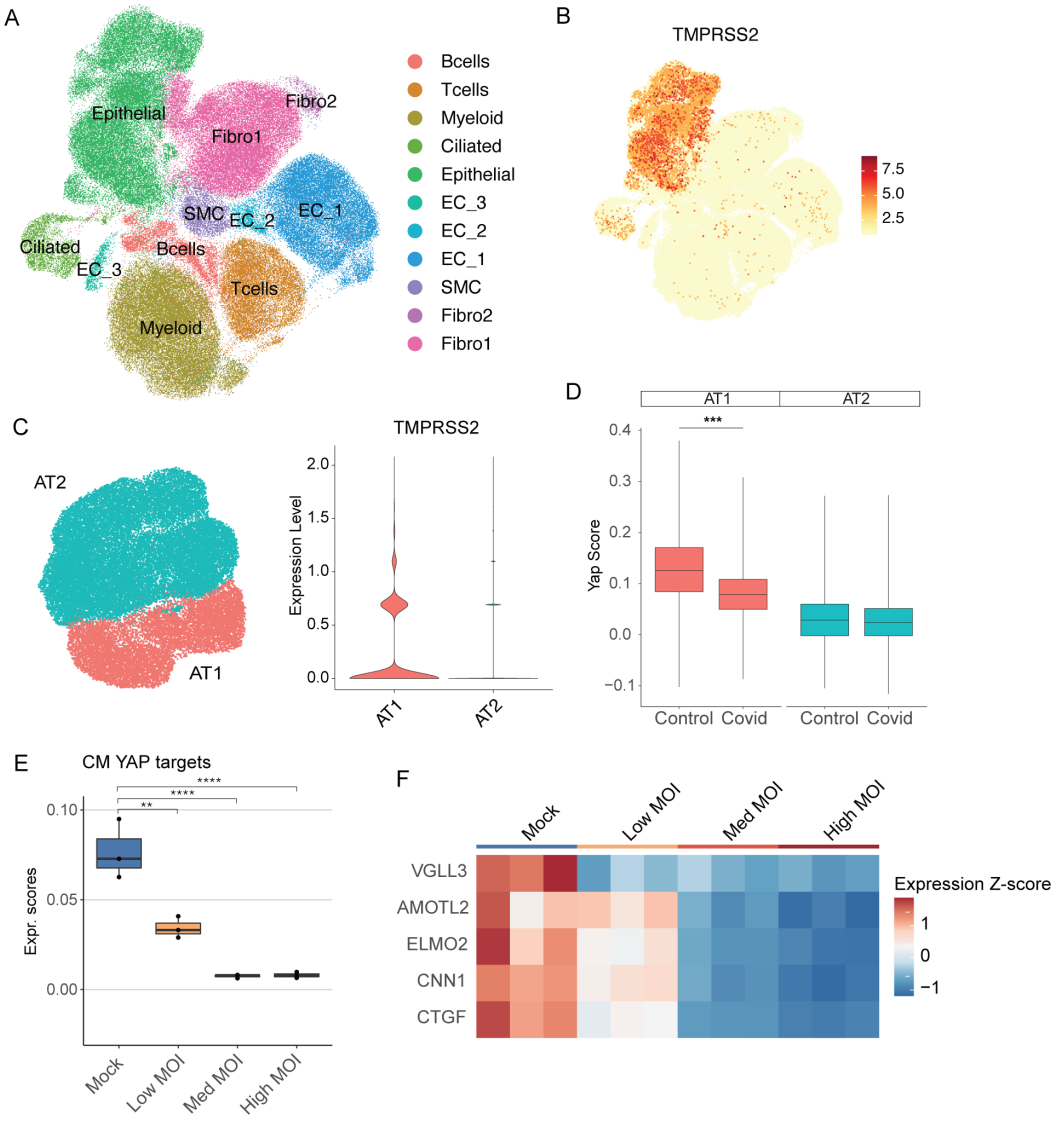

Figure 2. NSP13 inhibits YAP in vitro and in vivo.

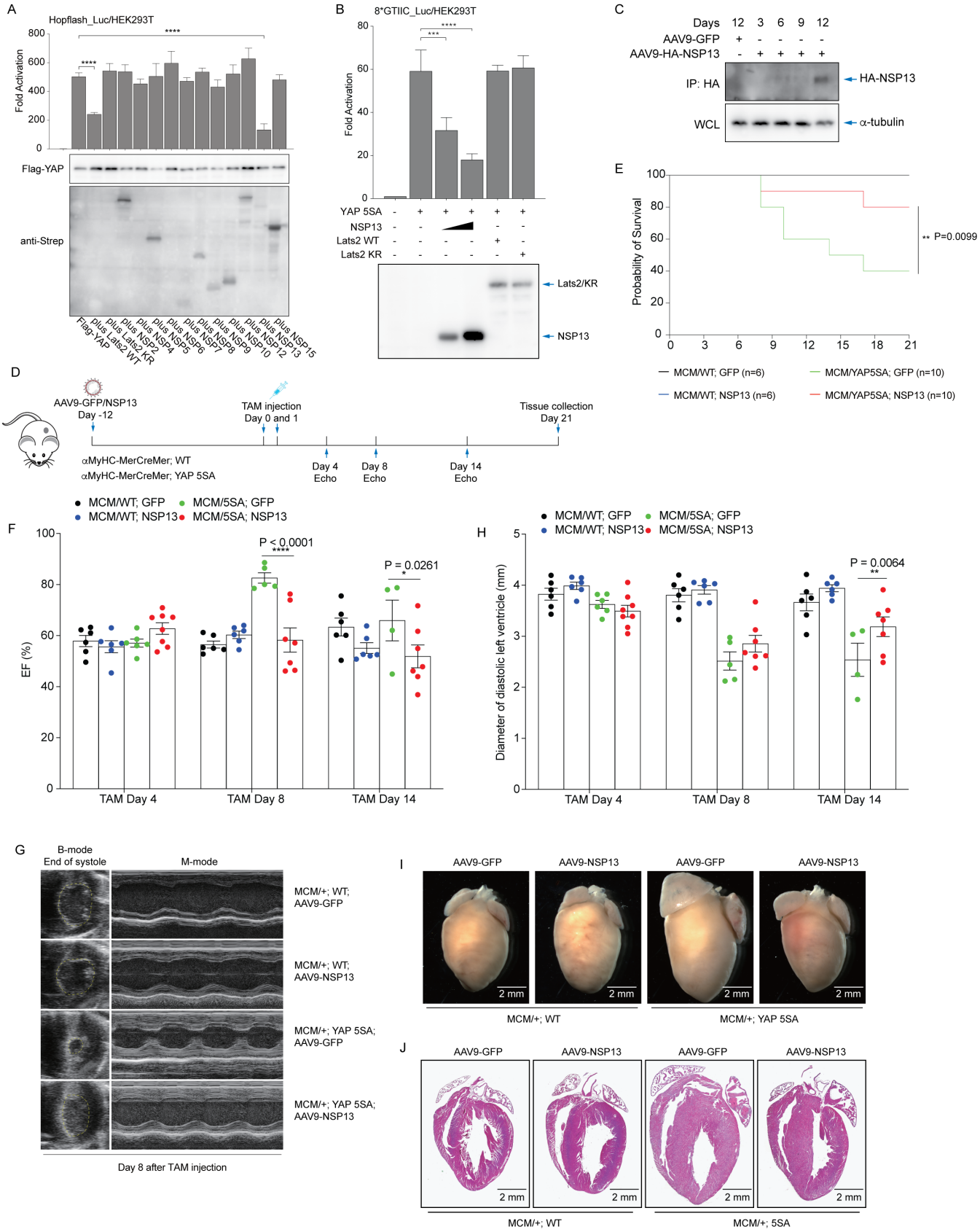

Figure 3. NSP13 suppresses YAP activity depending on its helicase activity.

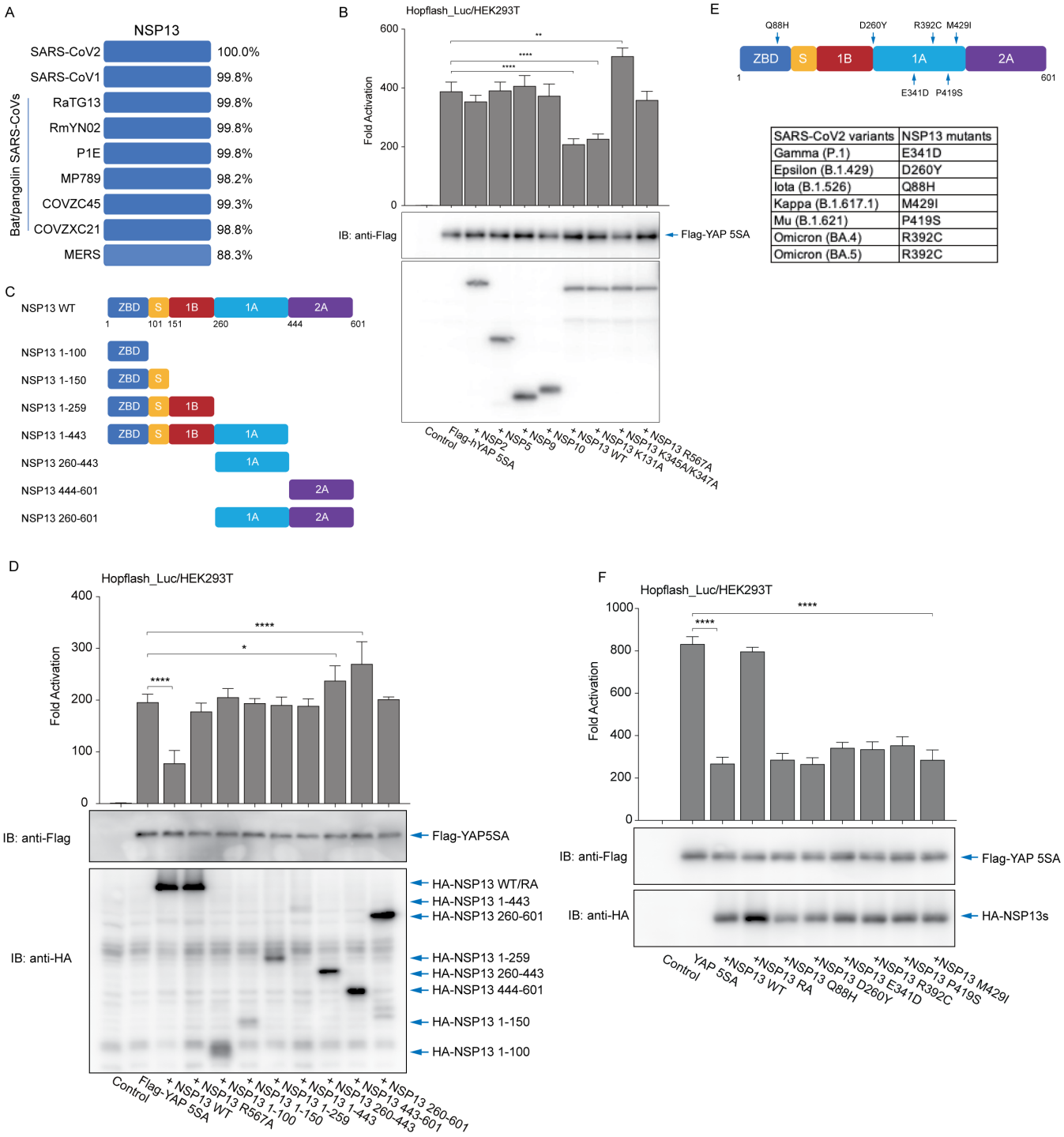

SARS-CoV2 variants	NSP13 mutants
Gamma (P.1)	E341D
Epsilon (B.1.429)	D260Y
Iota (B.1.526)	Q88H
Kappa (B.1.617.1)	M429I
Mu (B.1.621)	P419S
Omicron (BA.4)	R392C
Omicron (BA.5)	R392C
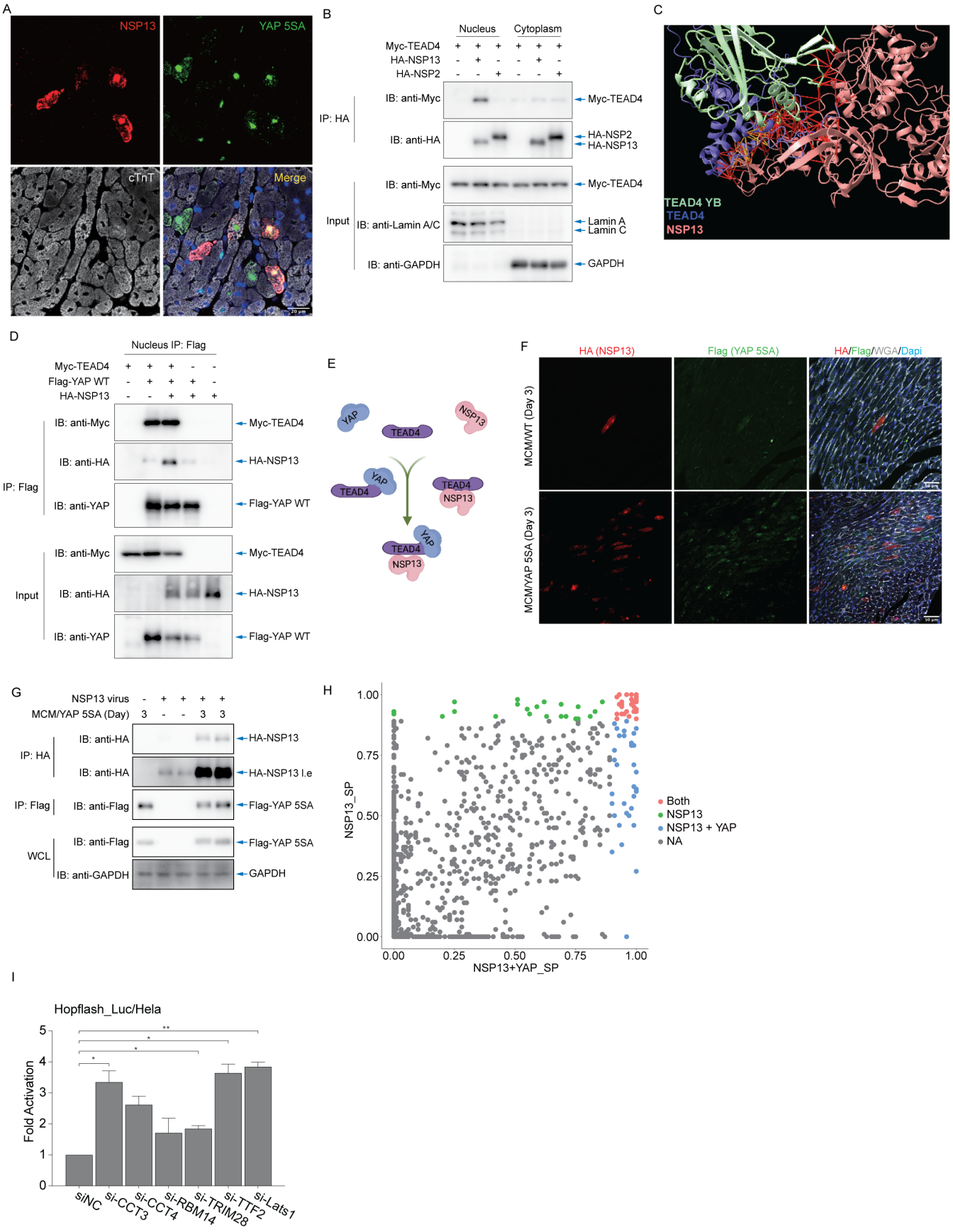
Figure 4. NSP13 inactivates YAP/TEAD4 complex by recruiting YAP suppressors.